



Lawrence Berkeley Laboratory

UNIVERSITY OF CALIFORNIA

Materials & Molecular Research Division

RECEIVED
LAWRENCE
BERKELEY LABORATORY
JUL 17
LIBRARY
DOCUMENTS

EFFECT OF VANADIUM ON DUAL PHASE Fe/Mn/Si/0.1C STEELS

Alvin H. Nakagawa
(M.S. thesis)

June 1981

TWO-WEEK LOAN COPY

This is a Library Circulating Copy
which may be borrowed for two weeks.
For a personal retention copy, call
Tech. Info. Division, Ext. 6782



LBL-12843
c.2

DISCLAIMER

This document was prepared as an account of work sponsored by the United States Government. While this document is believed to contain correct information, neither the United States Government nor any agency thereof, nor the Regents of the University of California, nor any of their employees, makes any warranty, express or implied, or assumes any legal responsibility for the accuracy, completeness, or usefulness of any information, apparatus, product, or process disclosed, or represents that its use would not infringe privately owned rights. Reference herein to any specific commercial product, process, or service by its trade name, trademark, manufacturer, or otherwise, does not necessarily constitute or imply its endorsement, recommendation, or favoring by the United States Government or any agency thereof, or the Regents of the University of California. The views and opinions of authors expressed herein do not necessarily state or reflect those of the United States Government or any agency thereof or the Regents of the University of California.

EFFECT OF VANADIUM ON DUAL PHASE Fe/Mn/Si/0.1C STEELS

Alvin H. Nakagawa

Materials and Molecular Research Division, Lawrence Berkeley Laboratory
and Department of Materials Science and Mineral Engineering
University of California, Berkeley, CA 94720

ABSTRACT

This investigation is concerned with the effect of a 0.12% vanadium addition on a Fe/1.2Mn/0.6Si/0.1C dual phase steel. A comparison of structure and mechanical properties was made between these two alloys with and without vanadium. Two phase ($\alpha + \gamma$) and single phase (γ) annealing treatments were followed by a wide range of cooling rates.

In most cases, vanadium did not have a significant beneficial effect on the mechanical properties, although it changed the microstructure. The vanadium addition caused precipitation of vanadium carbide in the ferrite and a decrease in the ferrite grain size. During air cooling from the austenite phase field, it caused a small amount of martensite to form in an otherwise ferrite and pearlite microstructure. The precipitation strengthening effect of the vanadium carbides may have been too small to counteract the decrease in the amount of carbon strengthening of the martensite in the vanadium containing alloy. Oil quenching from the austenite phase field, gave the best mechanical properties for both the nonvanadium and the vanadium bearing steels. In the latter case, the microstructure consisted of lath martensite plus bainitic ferrite-type structures.

This research was supported by the Division of Materials Sciences, Office of Basic Energy Sciences of the U.S. Department of Energy under Contract No. W-7405-ENG-48.

I. INTRODUCTION

The need for a strong formable steel for the automotive industry has been the driving force for numerous alloy development programs. One of the results has been the development of low carbon dual-phase (duplex ferrite-martensite) steels. Dual-phase structures can be produced by annealing in the ($\alpha + \gamma$) region followed by cooling rates sufficient to transform the austenite to martensite^{1,2}. Other industrial type processing of dual phase steels include hot rolling, continuous annealing, batch annealing³, and continuous cooling from the austenite region⁴. As opposed to grain size control and carbide precipitation in HSLA steels, the major source of strengthening in the dual-phase steels is the incorporation of strong martensite in a ductile ferrite matrix⁵.

The characteristics of dual phase steels are low yield strength to tensile strength ratios, continuous yielding behavior, high strain hardening rates and good ductility. The first two characteristics result from the large amount of fresh dislocations produced during the austenite to martensite transformation which occurs during cooling from the two phase region^{4,6}. During tensile testing or forming deformation, continuity of strain between the hard martensite and soft ferrite requires that there be large amounts of inhomogeneous deformation in the ferrite. This causes a further increase in the dislocation density in the ferrite near the martensite and the results in a high rate of work hardening^{4,6}. The transformations of any retained austenite also increases the number of dislocations⁶ and the work hardening rate⁷. The high rate of work hardening suppresses necking, resulting in excellent uniform elongation values which in turn increases the total elongation^{4,6}.

Since the study of dual-phase steels was started here at Berkeley by

Thomas and Koo², the effects of different metallurgical variables such as martensite volume fraction⁸, morphology⁹, carbon content⁸, and alloying additions^{10,11,12} have been studied.

In this investigation, the effect of a strong carbide forming element viz. vanadium on a dual phase steel has been studied. The main objective is to determine its effect on tensile properties because of anticipated effects on the microstructure and hence to establish structure property relationships. In all of the above cases, the effect of vanadium was isolated in several different heat treatments by comparing the vanadium containing alloy with an identical alloy without vanadium. Besides the fundamental research reasons for this investigation, there are economic and resource conservation reasons for determining whether or not vanadium is a necessary alloying addition in this dual phase steel.

II. EXPERIMENTAL PROCEDURE

A. Materials Preparation

The alloys used in this investigation were vacuum induction melted at Lawrence Berkeley Laboratory in the form of 20 pound cylindrical ingots. The ingots were homogenized in argon at 1100°C for 24 hours. They were upset and cross-forged at 1100°C to 3" by 1" bars and then hot rolled at 1100°C to approximately 1/8". All of the above treatments were followed by air cooling. Oversized tensile blanks were cut from the flat plate with the tensile axis parallel to the rolling direction.

The chemical compositions of the two alloys as analyzed by wet chemical (C and Si) and X-ray spectroscopy (Mn and V) are given in Table 1.

B. Heat Treatment

The hot rolled specimens were heat treated in a vertical tube furnace

under a flowing argon atmosphere. Four specimens were heat treated at the same time in a holder that kept them evenly spaced at right angles. Three specimens were used for tensile testing and the fourth was cut into pieces for optical, TEM and X-ray studies. The specimens were either intercritically annealed in the alpha + gamma phase field at 800°C or in the gamma region at 900°C. As shown in Fig. 1(a), the specimens were heated up to within 5°C of their final temperature after about 7 minutes. After a total holding time of 10 minutes, the specimens were dropped through the bottom of the furnace and subjected to either an agitated iced brine quench, an agitated oil quench, a forced air cool or a natural convection air cool.

The corresponding cooling rates from 800°C were measured by a thermocouple in the center of the specimen and recorded by a strip chart recorder. The results appear in Fig. 1(b). The average cooling rates from 800°C to 400°C for the iced brine quench, oil quench, forced air cool and air cool were found to be approximately 1000°C/sec, 100°C/sec, 5°C/sec and 3°C/sec respectively. The cooling rates from 900°C were found to be in the same range.

The calculated M_s temperature for the alloys is 465°C¹³. When the alloys are held at 800°C, the microstructure is approximately 20% austenite. Assuming that the carbon is enriched to 0.5%, the calculated M_s temperature becomes 350°C.

C. Mechanical Testing

Tensile properties were determined using 0.1" flat tensile bars with 1" gauge lengths. After heat treating, the oversize specimens were ground under flood cooling to ASTM specification E8-69 shown in Fig. 2. The

specimen thickness is 0.100". Approximately 35 mils of material was ground from the surface of the specimens to remove any decarburized material. The decarburization was less than 25 mils.

Testing was done at room temperature on an Instron testing machine with a cross-head speed of 0.05/min and a full scale load of 1000kg. The total elongations were determined by measuring 1" marks on the gauge before and after testing. The reduction in area was based on measurements of the gauge dimensions before and after testing with a micrometer and then an optical microscope equipped with a vernier translating stage. The rest of the properties were determined from the curves produced by the testing machine's chart recorder. The yield strengths were determined by the 0.2% offset method.

D. Metallography

1. Optical Metallography. Specimens for optical metallography were cut from the extra tensile blanks under flood cooling. After mounting in either bakelite or kold-mount, they were rough ground on a flood cooled 240 grit belt and then hand ground on wet silicon carbide paper from 240 to 600 grit. The final polish was done with 1 μ m diamond paste on a polishing wheel and then with 0.3 μ m alumina on a felt cloth. After the microstructural details were revealed by etching in a 2% nital solution, the specimens were observed in a Zeiss Ultraphot II metallograph. Volume fractions were determined by a point fraction method¹⁴.

2. Transmission Electron Microscopy. Thin foils for transmission electron microscopy were obtained from part of the extra tensile blank. Slices of approximately 25 mils were slow cut with a 1/32" silicon carbide abrasive disc under flood cooling. The slices were then given a uniform

thickness by removing 0.5 mils per pass with a flood cooled surface grinder. The slices were chemically thinned to 2-3 mils at room temperature in a solution of 96 ml of 30% H_2O_2 and 4 ml of 48% HF. After the 3 mm discs were spark cut from these slices, they were hand ground on 600 grit to remove any oxide layer. The discs were polished to thin foils at room temperature in a twin jet electropolisher using a chromic acetic acid solution of 75 gm CrO_3 , 400 ml CH_3COOH and 21 ml distilled water. Polishing potentials from 35-50 volts were used. The thin foils were stored in 200 proof ethyl alcohol and later examined in a Hitachi HU125 or a Philips EM301 electron microscope at an accelerating voltage of 100 kV. STEM analysis was done with a Philips EM400 electron microscope.

3. Scanning Electron Microscopy. Fractography was conducted on the broken surfaces of the tensile specimens using an AMR-1000 scanning electron microscope operating at 20 kV. The gauge sections of the specimens were removed with a hand saw and clamped in a specimen holder for observations.

E. X-ray Analysis

X-ray diffraction was used to determine the volume fraction of retained austenite in the steels. Part of the extra tensile blanks were used for this purpose. A surface grinder with flood cooling was used to remove 25 mils from each side. The specimens were then wet ground on silicon carbide paper from 240 to 600 grit. One side was chemically thinned at room temperature in a solution of 96 ml of 30% H_2O_2 and 4 ml of 40% HF while the other side was protected by a lacquer.

The resulting shiny surface was examined with a General Electric Diano X-ray diffractometer using filtered $Mo K_{\alpha}$ radiation. The specimens

were scanned at 0.2°/min from $2\theta = 20^\circ$ to $2\theta = 40^\circ$ to include the γ_{200} , α_{200} , γ_{220} , α_{211} and γ_{311} peaks following the procedure outlined by Miller¹⁵. The specimens were examined with their rolling directions both parallel and perpendicular to the X-ray beams.

III. Results and Discussion

A. Microstructure

1. Effect of Heat Treatment. A summary of the optical and TEM observations of the microstructures appears in Table II. The starting microstructures (as hot rolled) for the two steels are shown in Fig. 3. They consist mainly of proeutectoid ferrite plus a second phase or pearlite. The grain size is approximately the same in the two steels. The only difference between the two is the banding in the base steel (MB).

When the steels are heated to 800°C, the austenite nucleates heterogeneously at Fe_3C particles located on ferrite/ferrite grain boundaries¹⁵, then grows to approximately 20% of the total volume as determined by the tie line in the $(\alpha + \gamma)$ region of the iron-carbon-manganese equilibrium phase diagram. The actual amount is slightly less than equilibrium because of the short annealing time. It is not necessary to know the boundaries of the $(\alpha + \gamma)$ phase field since the annealing temperature for a specific volume fraction can be determined by a few test samples.

Quenching in agitated iced brine (800°C IBQ) transforms the austenite which forms during the annealing into martensite as can be seen in Fig. 4. The fine globules of martensite decorate the ferrite grain boundaries. The austenite grows along the boundaries rather than into the ferrite grains since carbon diffusion is much more rapid parallel to rather than

perpendicular to grain boundaries¹⁶. Figs. 5 and 6 show the high concentration of dislocations at the ferrite/martensite interface that are typical in dual-phase steels. In Figure 5 one can see the two regions of ferrite in alloy MV. Near the martensite there is a precipitate free area with a high density of dislocations. Further into the ferrite, there are less dislocations in the precipitate hardened area.

The martensite consists of lath and some twinned martensite. The presence of twinned martensite is to be expected since the carbon content is greater than 0.4%¹⁷.

Oil quenching from 800°C (800°C OIL) produces the microstructure shown in Fig. 7. The volume fraction and distribution of martensite is nearly the same as above.

Upon forced air (800°C FAC) and natural convection air cooling (800°C AC) from 800°C, the austenite which forms during two phase annealing transforms to additional proeutectoid ferrite and then to pearlite and maybe some upper bainite but no martensite or lower bainite. The resulting microstructures are shown in Fig. 8. When the steels are heated to 900°C, the austenite nucleates and grows to nearly 100% of the total volume since 900°C is in the austenite phase field for the compositions used.

Quenching in oil (900°C OIL) causes some proeutectoid ferrite to form. The remaining austenite then transforms to martensite to give the microstructures shown in Fig. 9. Although most of the second phase consists of lath martensite, there is also a small amount of bainite as shown in Fig. 10. Upon forced air (900°C FAC) and natural convection air cooling (900°C AC) from 900°C, pearlite formation again follows the formation of proeutectoid ferrite. The microstructures for 900°C AC are shown in Fig. 11.

Figs. 12 and 13 show the pearlite and surrounding ferrite. Considerable precipitation is visible in the proeutectoid ferrite of Fig. 12, but the ferrite in Fig. 13 appears to be much "cleaner". Fig. 14 is a TEM micrograph of the MB 900 AC steels showing the fine precipitates found in varying amounts in all of the specimens. The microstructures of the 900°C AC specimens are similar to those of the 800°C AC treatment except that all of the ferrite forms during cooling since no ferrite can be retained during annealing in the austenite range. In the forced air and air cool treatments from both 800°C and 900°C, the volume fraction of the pearlite is approximately 10%.

2. Effect of Vanadium. In steels, vanadium tends to form carbides, the equilibrium form being V_4C_3 . Besides increasing the strength of the ferrite by precipitation hardening, other effects of vanadium are to increase the hardenability and to reduce the austenite grain size¹⁸. Hardenability is increased by the competition of the formation of vanadium carbide with that of cementite, thus retarding higher transformation temperature products. Vanadium carbides cause smaller austenite grain sizes during controlled rolling by providing more nucleation sites for recrystallization and by retarding grain growth.

Although vanadium is known to be an effective grain refining alloying addition, it does not seem to have much of an effect on the grain size of the as-received (hot rolled) material as shown in Fig. 3. However, the optical micrographs of the heat treated steels, Figs. 4, 7-9 and 11, show the effectiveness of vanadium in causing a smaller grain size.

For example, in the 800°C iced brine quench specimen, Fig. 4, the austenite (martensite) and ferrite grains are noticeably smaller in

vanadium containing alloy (b). Since the austenite grains are surrounded by ferrite during two-phase annealing, grain growth in the usual sense (e.g. austenite grain boundary motion) cannot occur. Instead, a coarsening reaction would have to take place. In this case, the effect of the vanadium is to reduce the diffusivity of carbon because of its carbon affinity and size difference with respect to iron. The result is a decrease in the rate of the coarsening reaction.

In the case of the ferrite, there are many ferrite/ferrite grain boundaries. In the alloy without vanadium, there are fewer austenite particles as a result of the coarsening reaction and there are no VC precipitates. This allows the ferrite/ferrite grain boundaries to move freely causing the ferrite grains to be larger in the alloy without vanadium as shown in Fig. 4.

During 900°C annealing, the microstructure consists of only austenite, thus reduction of austenite grain growth during annealing and increased ferrite nucleation during cooling are probably the mechanisms by which vanadium caused the smaller grain sizes in alloy MV as compared to MB after 900°C annealing. The nucleation of austenite during heating and renucleation of ferrite during cooling together with the effect of vanadium account for the smaller grain size of the vanadium containing alloy after heat treatment as compared to the as received material.

In the transmission electron microscope, one can see that vanadium causes significant differences in the precipitate morphology. Fig. 15 shows the interphase precipitation found only in the vanadium containing alloy. It is well known that carbide forming elements such as vanadium promote

this type of precipitation¹⁹. Another difference is shown in Fig. 16. In addition to the pearlite found in the 900°C AC specimens, some twinned plate martensite was found in the vanadium containing alloy. This may be due either to the hardenability effect of vanadium or to some segregation of manganese or carbon caused by the vanadium. Although the fine precipitates shown in Figs. 12 and 14 were found in all of the treatments, the density of the precipitates was much higher in the vanadium containing alloys. No difference was found between the two alloys in the 900°C OIL heat treatment.

Table II summarizes the effect of vanadium on the microstructure of the steel.

STEM analysis of the vanadium containing alloy with the 800°C iced brine quench heat treatment did not detect any vanadium partitioning between the ferrite and martensite. This was probably because the amount of vanadium in the alloy (0.13 at %) was below the detectability level for the instrument.

3. Fractography. A SEM micrograph of the dimpled structure of the tensile specimen fracture surface appears in Fig. 17. This is for the 800°C IBQ treatment, but the ductile fracture appearance is typical of all the specimens tested.

4. Retained Austenite. There have been several reports of retained austenite in dual-phase steels^{3,6,16,20-24}. The reported amounts of retained austenite vary from less than 1%¹⁶ to as much as 12.6%²³ with most reporting approximately 5% for compositions similar to the one being studied. The volume percent was found to increase with the annealing temperature^{3,24} and the concentration of vanadium²³. The cooling rate

may have an effect, but it has not been well established. One report found that the amount of austenite increased with decreasing cooling rates²³ while another reported a maximum in the volume percent at a cooling rate of 50°C/sec.⁶ There have been reports of thermally stable^{20,21} as well as thermally unstable^{22,23} retained austenite. In most cases, it was not found to be mechanically stable. The effect on mechanical properties is also unclear. One report concluded that the amount is too small to have any effect²⁴ and another found that it transforms too easily to have any effect²². On one hand, it was concluded that the ductility increases with the volume percent of retained austenite²³ and on another that the strain hardening rate increased with the amount of retained austenite²¹.

X-ray analysis of the vanadium containing alloy after all five heat treatments failed to detect any retained austenite. No X-ray analysis was done on the alloy without vanadium. TEM studies also failed to reveal any retained austenite in either alloy. Thus in the present investigation it can be concluded that if there is retained austenite the amount must be less than ~1%.

In this investigation, the retained austenite volume fraction may have been too low to detect by X-ray diffraction because of the heat treatment used. It is possible that the discrete particle retained austenite which was reported in the literature results from a high degree of partitioning of carbon and manganese, both of which are austenite stabilizers²⁵⁻²⁷. Furukawa et al.²¹ purposely obtained an enriched second phase prior to heat treatment by careful control of the coiling temperature following the hot rolling treatment. The short annealing time (2 minutes) and low annealing temperature (750°C) used in that

investigation helped maintain the segregation in the austenite. Upon cooling, some of this enriched austenite is retained. This investigation used a simple hot rolling and a 10 minute anneal at 800°C or 900°C. Some investigators^{6,28} reporting retained austenite in their dual-phase steel used a neutral salt pot for their heat treatments which gives a much more rapid heating rate than the tube furnace used in the present investigation. This would result in a higher nucleation rate for the austenite, thus resulting in a large number of small austenite particles. It has been speculated that these particles are stabilized and therefore retained because of their small size through restraint or lack of nucleation site.

B. Mechanical Properties

1. Effect of Heat Treatment. A summary of the tensile test data appears in Table III. For each heat treatment, the data is given for the base alloy (MB) and the vanadium containing alloy (MV): There is a third row designated by Δ_V which indicates the changes in mechanical properties due to the addition of vanadium.²⁹

For steels given the 800°C annealing treatment, one can see the effect of different cooling rates on dual-phase steels. As the cooling rate decreases from iced brine quench, to oil quench, to air cool, there is as expected, a decrease in the ultimate tensile strength (from ~ 110ksi down to ~ 80 ksi) and an increase in total elongation (from ~20% up to ~30%). The uniform yielding characteristics give way to the undesirable Lüders strain as the second phase changes from martensite to pearlite. Somewhere between cooling rates of 100°C/sec and 5°C/sec, the volume fraction of martensite goes below the minimum requirement of 10% for

continuous yielding behavior³. There is a decrease in the yield strength following iced brine quench compared to oil quenching, because the slower cooling rate reduces the hardening effect of the interstitial carbon²¹, but the yield strength rises for the air cooling treatments because there no longer is any martensitic transformation to produce the fresh, mobile dislocations expected from the transformation strain.

The change to the higher annealing temperature from 800°C to 900°C results in a higher strength upon oil quenching (from ~ 90ksi up to ~ 115ksi) and lower values of elongation (from ~ 28% down to ~ 23%). The results of this 900°C OIL treatment are rather interesting because although oil quenching from the austenite region is unlike any conventional dual-phase treatment, it yields better values of both strength and ductility than the 800°C IBQ treatment. Of all the treatments used, this one gave the highest value of UTS x Total elongation.

In comparing the 900°C OIL to the 800°C OIL results, the increase in strength comes from the increase in the volume fraction of martensite. The higher values of ductility than expected for such a large volume fraction of martensite result from the change in the martensite morphology as the austenite carbon content changed from 0.5% to 0.1%. The 800°C IBQ specimen contained a mixture of lath and twinned martensite, while the 900°C OIL specimen contained a mixture of lath martensite and upper bainite. The small amount of proeutectoid ferrite also added to the ductility.

2. Effect of Vanadium. A comparison of the stress strain curves for steels with and without vanadium appears in Fig. 18. Overall, the effect of vanadium is not significant in the heat treatments used. The

two minor exceptions are the 800°C IBQ and 800°C OIL treatments. In 800°C IBQ, (Fig. 18(a)), the yield and tensile strength is lowered by 7 ksi and 9 ksi respectively, while the elongations remain the same. In 800°C OIL, (Fig. 18(b)), the effect is the opposite. The yield and tensile strengths increase 7 ksi and 10 ksi respectively while the elongations decrease by approximately 5%.

One possible cause for the lower tensile strength of the vanadium containing alloy in the 800°C IBQ treatment is the lower amount of carbon available for the major strengthener, the martensite. A small factor contributing to this lower amount is the overall carbon content of the alloys. As shown in Table 1, the alloy without vanadium has 0.12% carbon, while the vanadium containing alloy has only 0.1% carbon. However, this effect is small since the 0.02 weight percent difference results in only a 4% change in the volume fraction of martensite at the same 800°C annealing temperature. Using the law of mixtures⁸ as a guide, a rough calculation approximates the change in strength as 5 ksi. The effect is probably much less.

The effect of the vanadium is much greater. The first effect is on the phase diagram. Vanadium expands the ($\alpha + \gamma$) phase field since it is a ferrite former and it depresses the a_{c1} by 50°C per 1% V³⁰. These changes affect the volume percent as well as the composition of the martensite. The second effect is the decrease in solid solution carbon content due to the carbon formation of vanadium carbides. This is probably the major cause of the lower strength in the 800°C IBQ treatment.

Normally, one would expect the strength to increase because of the vanadium carbides. The increase may have been too small to overcome the

loss in strength caused by the decrease in carbon because of coarse carbides left from hot rolling.

In the 800°C OIL treatment, the slower cooling rate may have allowed more time for the formation of carbides and strengthened proeutectoid ferrite. This increased the strength of the vanadium containing alloy efficiently enough to overcome the lower carbon level.

In the 800°C AC data, one can see that the yield strength of the vanadium containing alloy is higher than that of the base alloy. This is probably due to the increased precipitation in the ferrite. The lower yield strength of the vanadium containing alloy in the 900°C AC data may be due in part to some mobile dislocations in the ferrite originating from the strain associated with the transformation of austenite to a small amount of martensite in the vanadium containing alloy.

The key point is that a vanadium addition is not necessary to achieve superior tensile properties for the 900°C OIL treatment. The alloy without vanadium has properties that are essentially identical to those of the vanadium-containing alloy.

IV. Conclusions

Based on the present investigation of the effect of a 0.12%V addition on a dual-phase Fe/Mn/Si/0.1C alloy, the following conclusions can be drawn:

1. The addition of 0.12%V caused a decrease in the ferrite grain size, caused interphase precipitation of carbides, caused an increase in the density of fine precipitates in the ferrite and, in air cooled specimens, caused the formation of a small amount of martensite in the otherwise pearlitic structure.

2. However, despite the changes in microstructure, the vanadium addition did not cause any significant beneficial effect on the tensile properties.
3. The precipitation strengthening of the vanadium containing alloy may have been counteracted by the lower volume fraction of martensite and the lower amount of soluble carbon available in martensite because of the carbon tied up in the precipitates.
4. The 900°C oil quench treatment produced the best properties even though quenching in oil from the austenite phase field is not a conventional dual-phase heat treatment.
5. In this superior heat treatment, the properties and microstructures of the two alloys were almost identical.
6. Air cooling and forced air cooling from the two phase ($\alpha + \gamma$) region and the single phase austenite region produced a predominantly ferrite plus pearlite microstructure with undesirable discontinuous yielding.

ACKNOWLEDGEMENTS

The author gratefully acknowledges the support, encouragement and guidance of Professor Gareth Thomas throughout the course of this investigation. The assistance and discussions of Dr. J. Y. Koo and N. J. Kim proved to be invaluable. Thanks are also due to Professors I. Finnie and J. W. Morris, Jr. for reviewing this manuscript.

The assistance of the technical support staff of the Materials and Molecular Research Division of Lawrence Berkeley Laboratory is gratefully acknowledged. In particular, the assistance of John Holthuis,

Don Krieger and Weyland Wong is recognized.

Thanks are also due to Madeline Moore and Kathleen Brusse for typing this manuscript.

This research was supported by the Division of Materials Sciences, Office of Basic Energy Sciences, U.S. Department of Energy under Contract No. W-7405-ENG-48.

REFERENCES

1. M. S. Rashid, "GM980X - A Unique High Strength Steel with Superior Formability", SAE 760206, 1976.
2. J. Y. Koo and G. Thomas, "Thermal Cycling Treatments and Microstructures for Improved Properties of Fe-0.12%C-0.5%Mn Steels," Mat. Sci. and Eng. 24, 187 (1976).
3. J. M. Rigsbee, J. K. Abraham, A. T. Davenport, J. E. Franklin and J. W. Pickens, "Structure-Processing and Structure-Property Relationships in Commercially Processed Dual-Phase Steels", p. 304 in Structure and Properties of Dual-Phase Steels, R. A. Kot and J. W. Morris, eds., AIME, New York, N. Y. , 1979.
4. J. H. Bucher and E. G. Hamburg, "High Strength Formable Sheet Steel", SAE 770164, 1976.
5. J. Y. Koo and G. Thomas, "Design of Duplex Low Carbon Steels for Improved Strength: Weight Applications", p. 40 in Formable HSLA and Dual-Phase Steels, A. T. Davenport, ed., AIME, New York, N. Y., 1979.
6. D. K. Matlock, G. Krauss, L. F. Ramos and G. S. Huppi, "A Correlation of Processing Variables with Deformation Behavior of Dual Phase Steels", p. 62 in Structure and Properties of Dual-Phase Steel, R. A. Kot and J. W. Morris, eds., AIME, New York, N. Y., 1979.
7. D. Webster, "Development of a High Strength Stainless Steel with Improved Toughness and Ductility", Met. Trans. 2, 2097 (1971).
8. J. Y. Koo, M. J. Young, and G. Thomas, "On the Law of Mixtures in Dual-Phase Steels", Met. Trans. A 11A, 852 (1980).

9. N. J. Kim and G. Thomas, "Effects of Morphology on the Mechanical Behavior of a Dual-Phase Fe/2Si/0.1C Steel", Met. Trans. A 12A, 483 (1981).
10. P. K. Costello, "Design of Duplex Low Carbon Steels with Carbide Forming Elements", M. S. Thesis, University of California, Berkeley, LBL-8628, December 1978.
11. T. J. O'Neill, J. Y. Koo and G. Thomas, "Microstructure and Properties of Dual Phase Steels containing Silicon, Aluminum and Molybdenum, submitted to Met. Trans., November 1980.
12. J. S. Gau, "Mechanical Properties and Microstructure of a Low Carbon Steel with Nb.", M. S. Thesis, University of California, Berkeley, LBL-12058, April 1981.
13. R. E. Reed-Hill, Physical Metallurgy Principles, 2nd ed., D. Van Nostrand and Co., New York, 1973.
14. E. E. Underwood, "Applications of Quantitative Metallography", in ASM Metals Handbook, Vol. 8, p. 37 (1961).
15. R. L. Miller, "A Rapid X-ray method for the Determination of Retained Austenite", Trans. ASM 57, 839 (1964).
16. C. I. Garcia and A. J. DeArdo, "The Formation of Austenite in Low Alloy Steels", p. 40 in Structure and Properties of Dual-Phase Steels, R. A. Kot and J. W. Morris, eds., AIME, New York, N. Y., 1979.
17. B. V. N. Rao, "Role of Quaternary Additions on Dislocated Martensite Retain Austenite and Mechanical Properties of Fe/Cr/C Structural Steels," Ph.D. Thesis, University of California, Berkeley, LBL-7361, (1978).

18. J. F. Butler and J. H. Bucher, "Vanadium HSLA Steels with Superior Formability", in Production and Properties of Vanadium Dual Phase Steels and Cold Pressing Steels in the Automobile Industry, Proceedings of a seminar in Berlin, Vanadium International Technical Committee, October 1978.
19. R. W. K. Honeycombe, "Transformation from Austenite in Alloy Steels", Met. Trans. 7A, p. 915 (1976).
20. A. R. Marder, "Factors Affecting the Ductility of 'Dual-Phase' Alloys", in Formable HSLA and Dual-Phase Steels, A. T. Davenport ed., AIME, New York, N. Y., 1979, p. 89.
21. T. Furukawa, H. Morikawa, H. Takeuchi and K. Koyama, "Process Factors for Highly Ductile Dual-Phase Sheet Steels", p. 281 in Structure and Properties of Dual-Phase Steels, R. A. Kot and J. W. Morris, eds., AIME, New York, N. Y. 1979.
22. G. T. Eldis, "The Influence of Microstructure and Testing Procedure on the Measured Mechanical Properties of Heat Treated Dual-Phase Steels," p. 202 in Structure and Properties of Dual-Phase Steels, R. A. Kot and J. W. Morris, eds., AIME, New York, N. Y. 1979.
23. K. Nakaoka, Y. Hosoya, M. Ohmura and A. Hishimoto, "Reassessment of the Water-Quench Process as a Means of Producing Dual-Phase Formable Sheet Steels", p. 330 in Structure and Properties of Dual-Phase Steels, R. A. Kot and J. W. Morris, eds., AIME, New York, N. Y., 1979.
24. G. R. Speich and R. L. Miller, "Mechanical Properties of Ferrite-Martensite Steels," p. 145 in Structure and Properties of Dual-Phase

- Steels", R. A. Kot and J. W. Morris, eds., AIME, New York, N. Y., 1979.
25. P. G. Shewmon, Transformations in Metals, McGraw-Hill Book Co., New York, 1969.
 26. B. Edmondson and T. Ko, "Spontaneous Deformation of Austenite During Martensitic Transformations", Acta Met., 2, 235 (1954).
 27. K. W. Andrews, "The Calculation of Transformation Temperatures and Austenite-Ferrite Equilibria in Steels", JISI 184, 414 (1956).
 28. W. R. Cribb and J. M. Rigsbee, "Work-Hardening Behavior and its Relationship to the Microstructure and Mechanical Properties of Dual-Phase Steels", in Structure and Properties of Dual-Phase Steels, R. A. Kot and J. W. Morris, eds., AIME, New York, N. Y., 1979.
 29. W. C. Leslie and R. L. Miller, "The Stabilization of Austenite by Closely-Spaced Boundaries", Trans. ASM 57, 972 (1964).
 30. E. C. Rollason, "Fundamental Aspects of Molybdenum on Transformation of Steel", Climax Molybdenum Co., No. M89 12/72 IOM.

FIGURE CAPTIONS

- Fig. 1. Heating curve (a) and cooling curve (b) of specimens during heat treatment as measured by a thermocouple inside an extra tensile test blank.
- Fig. 2. Drawing of ASTM specification E8-69 flat tensile specimen. The specimen thickness is 0.100".
- Fig. 3. Optical microscopes of as received microstructure: (a) Base (MB), (b) Base + V (MV). Nital etch.
- Fig. 4. Optical micrographs of 800°C iced brine quench specimens: (a) Base, (b) Base + V. Nital etch.
- Fig. 5. TEM micrograph of MV 800°C IBQ showing dislocations in ferrite near martensite and interaction with precipitates.
- Fig. 6. TEM micrograph of MB 800°C IBQ showing dislocations in ferrite near martensite.
- Fig. 7. Optical micrographs of 800°C oil quench specimens: (a) Base, (b) Base + V. Nital etch.
- Fig. 8. Optical micrographs of 800°C air cool specimens: (a) Base, (b) Base + V. Nital etch.
- Fig. 9. Optical micrographs of 900°C oil quench specimens: (a) Base, (b) Base + V. Nital etch.
- Fig. 10. TEM micrograph of bainite in the MV 900°C oil quench specimen: (a) bright field and (b) SAD showing cementite [T00] with ferrite [T01].
- Fig. 11. Optical micrographs of 900°C air cool specimens: (a) Base, (b) Base + V. Nital etch.
- Fig. 12. TEM micrograph of pearlite in MV 900° AC with precipitation.

Fig. 13. TEM micrograph of pearlite surrounded by dislocation free ferrite in MB 900°C AC.

Fig. 14. TEM micrograph of precipitation in MB 900°C AC.

Fig. 15. TEM micrograph of interphase precipitation in MV 800°C IBQ.

Fig. 16. TEM micrographs of twinned martensite in MV 900°C AC.

Fig. 17. SEM micrographs of fracture surface of MB and MV 800°C IBQ tensile specimen.

Fig. 18. Stress strain curves comparing the base alloy (MB) with the alloy containing vanadium (MV) (a) 800°C iced brine quench, (b) 800°C oil quench, (c) 900°C oil quench, (d) 800°C air cool and (e) 900°C air cool.

Table I

Alloy Compositions (wt. pct.)

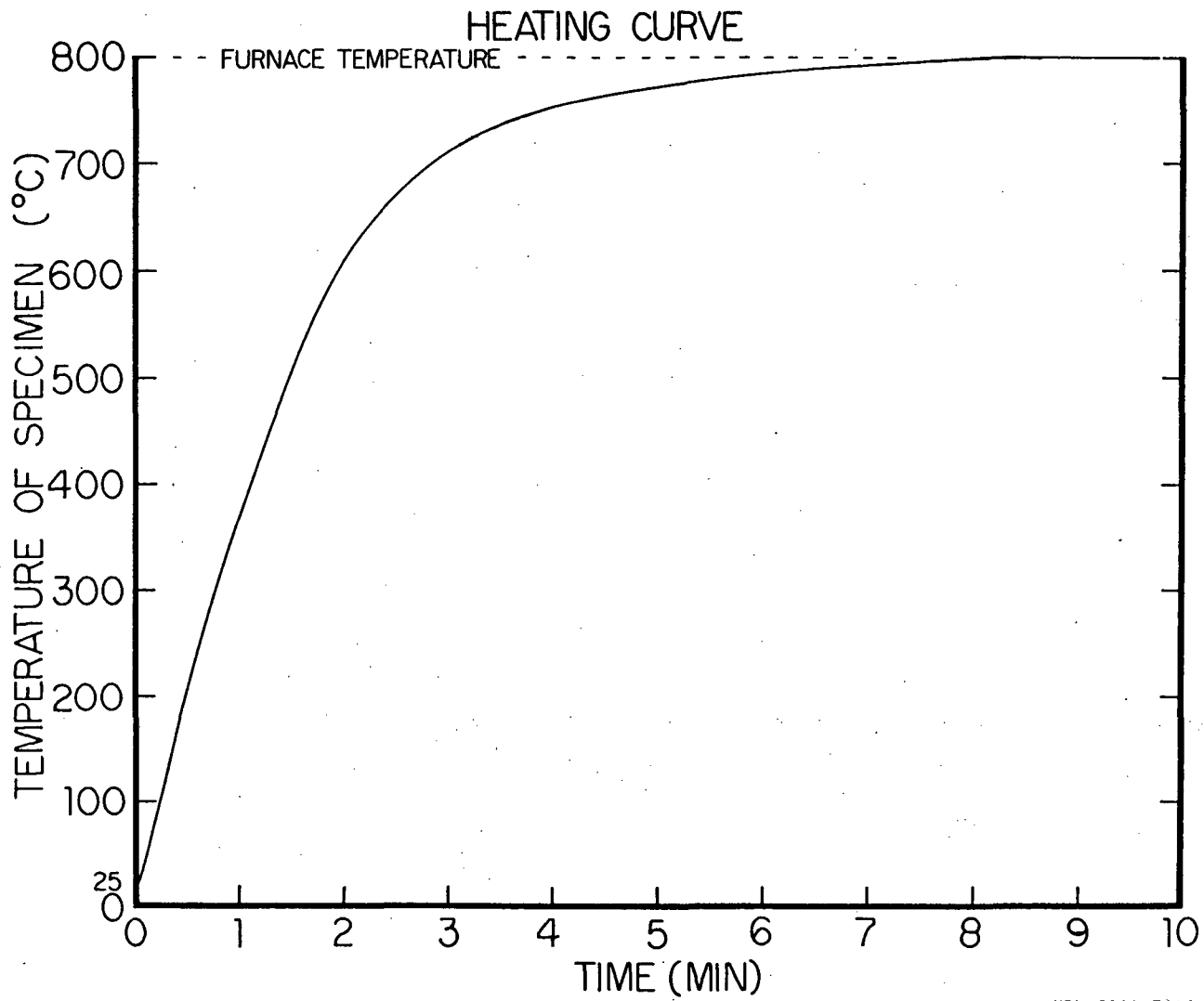
Alloy Designation	C	Si	Mn	V	Fe
MB	0.12	0.57	1.16	<0.005	Bal
MV	0.10	0.57	1.16	0.12	Bal

TABLE II Summary of Microstructures

Heat Treatment	Alloy	"Second Phase"	Interface Precipitation	Fine Precipitation (in ferrite(#/cm ³))	Type of ferrite
800IBQ	MB	Martensite	No	high 3.5 x 10 ¹⁵	retained +new
	MV	Martensite	Yes	very high 4.5 x 10 ¹⁵	retained
9000IL	MB	Martensite some upper bainite	No	low ~0	new
	MV	Martensite some upper bainite	No	low ~0	new
800AC	MB	Pearlite (upper bainite)	No	very low 200 2.5 x 10 ¹⁴	retained +new
	MV	Pearlite (upper bainite)	Yes	low 5 x 10 ¹⁴	retained +new
900AC	MB	Pearlite (upper bainite)	No	very low 2.5 x 10 ¹⁴	new
	MV	80% Pearlite+Bainite 20% Martensite	Yes	medium 2.0 x 10 ¹⁵	new

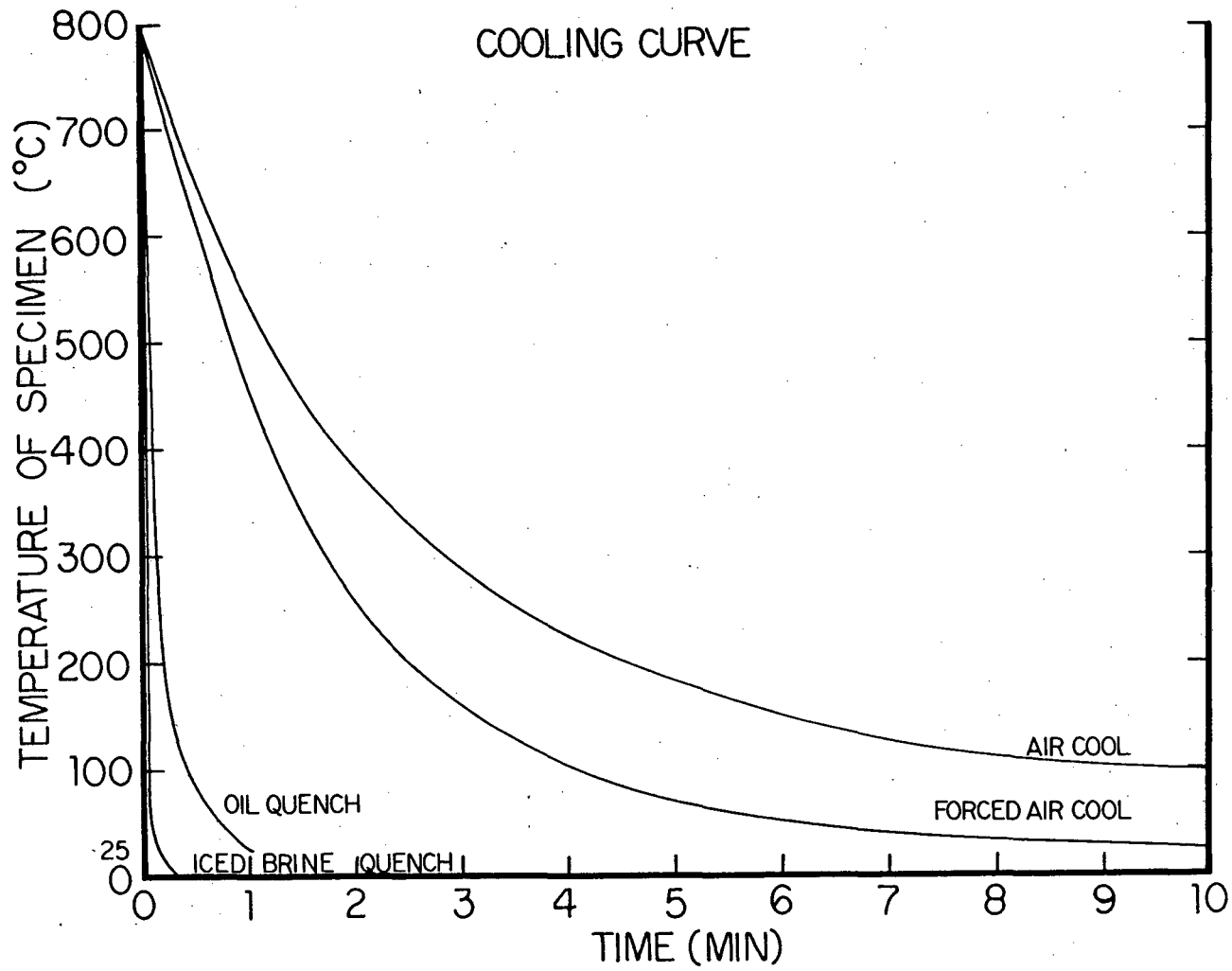
Table III
Tensile Properties

Heat Treatment	Alloy	Y.S. ksi (MPa)	U.T.S. ksi (MPa)	Y.S. / U.T.S.	Uniform Elongation (%)	Total Elongation (%)	Luders Strain (%)	Reduction in Area (%)	U.T.S. x Total Elong. ksi x % (GPa x %)
800°C IBQ	MB	65(448)	114(785)	0.57	13	19	0	50	2170(14.9)
	MV	58(400)	105(723)	0.55	13	19	0	54	2000(13.7)
	Δv	-7(-48)	-9(-62)	+0.02	0	0	0	+4	-170(-1.2)
800°C OIL	MB	47(324)	86(589)	0.55	23	30	0	41	2580(17.7)
	MV	54(369)	96(661)	0.56	17	25	0	47	2400(16.5)
	Δv	+7(+45)	+10(+72)	+0.01	-6	-5	0	+6	-180(-1.2)
900°C OIL	MB	77(531)	118(813)	0.65	12	22	0	75	2596(17.9)
	MV	79(544)	115(795)	0.68	12	23	0	71	2650(18.3)
	Δv	+2(+13)	-3(-18)	+0.03	0	+1	0	-4	+54(+0.4)
800°C FAC	MB	48(331)	76(521)	0.64	18	28	0.7	81	2130(14.6)
	MV	51(354)	76(526)	0.67	18	31	1.4	83	2360(16.3)
	Δv	+3(+23)	0(+5)	+0.03	0	+3	+0.7	+2	+230(+1.7)
900°C FAC	MB	56(386)	77(533)	0.72	19	33	2.5	84	2540(17.6)
	MV	56(386)	77(503)	0.77	21	36	3.2	84	2630(18.1)
	Δv	0(0)	-4(-30)	+0.05	+2	+3	+0.7	0	+90(+0.5)
800°C AC	MB	50(345)	77(531)	0.65	17	29	1.1	80	2230(15.4)
	MV	58(396)	75(517)	0.77	17	29	2.4	83	2180(15.0)
	Δv	+8(+51)	-2(-14)	+0.12	0	0	+1.3	+3	-50(-0.4)
900°C AC	MB	54(370)	75(517)	0.72	21	35	2.7	84	2630(18.1)
	MV	50(341)	76(520)	0.66	21	34	1.2	80	2580(17.7)
	Δv	-4(-29)	+1(+3)	-0.06	0	-1	-1.5	-4	-50(-0.4)



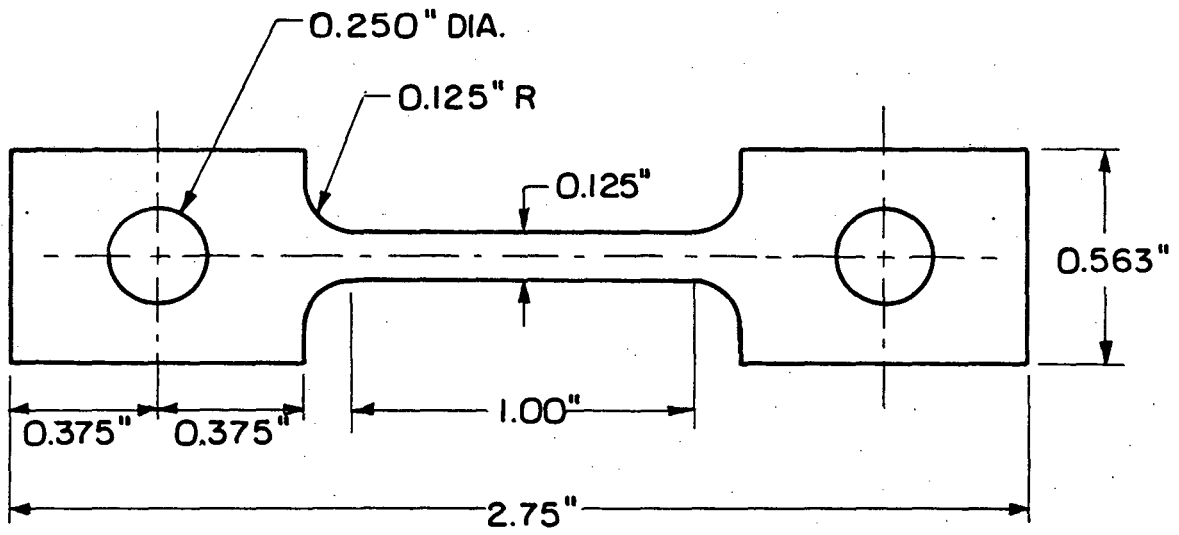
XBL 8011-7414

Fig. 1a



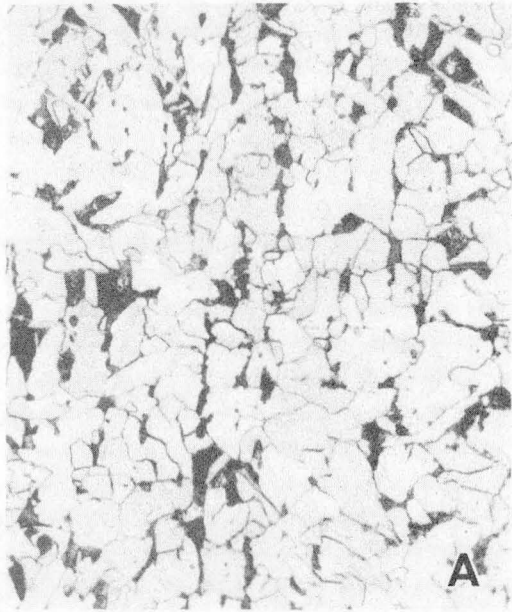
XBL 8011-7413

Fig. 1b

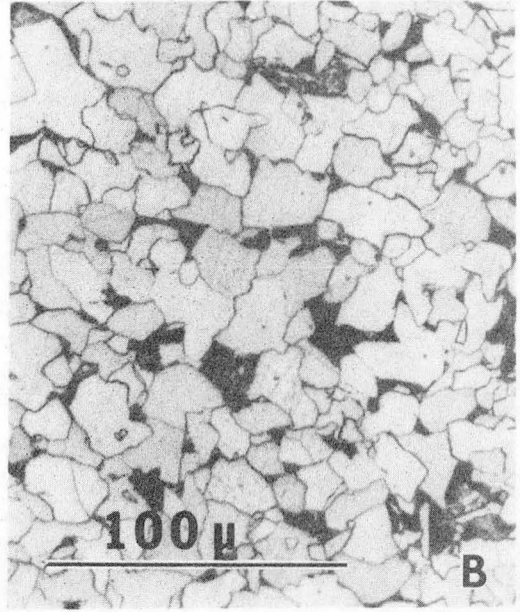


XBL737-6444

Fig. 2



BASE



BASE+V

AS RECEIVED

XBB 800-12387

Fig. 3

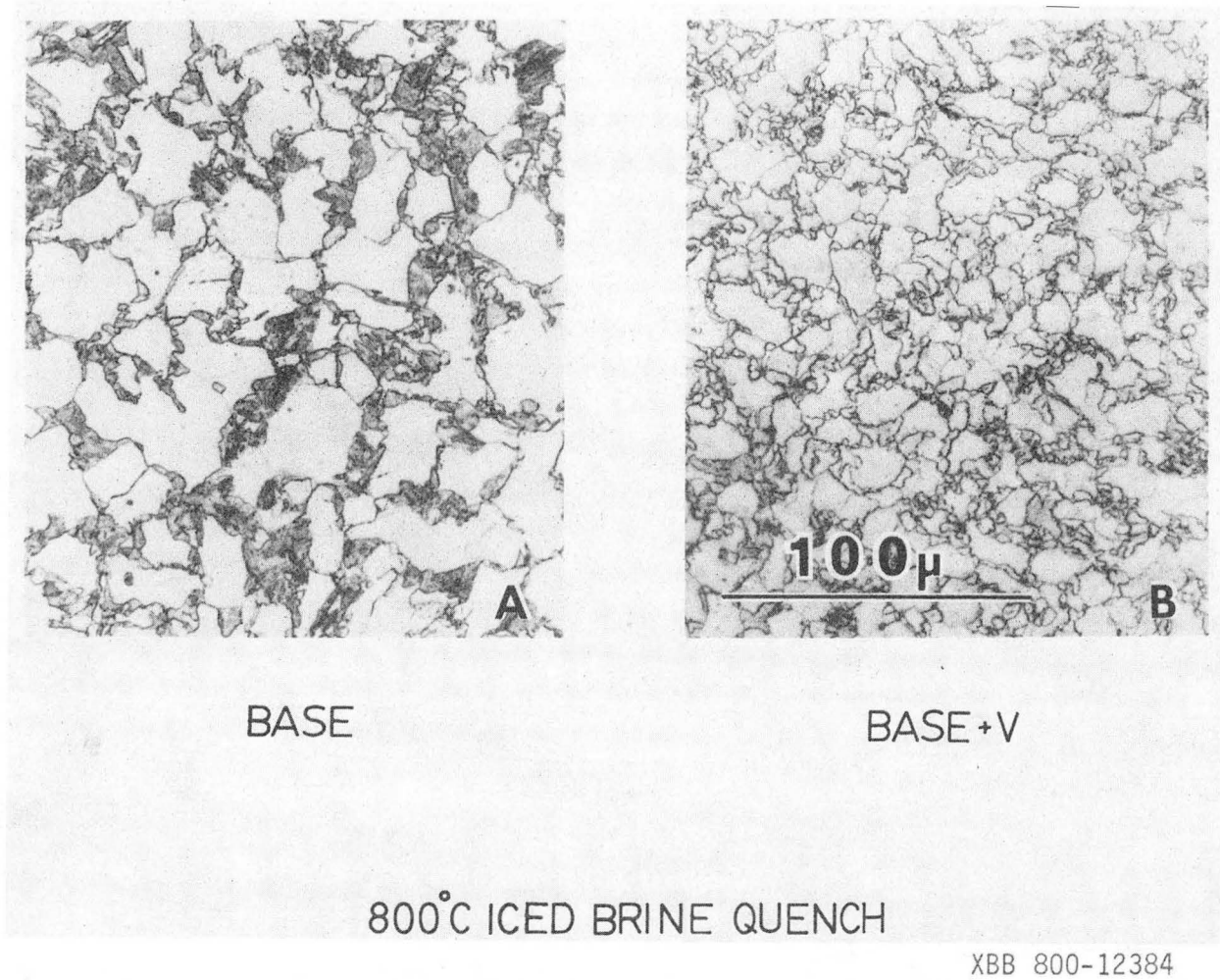
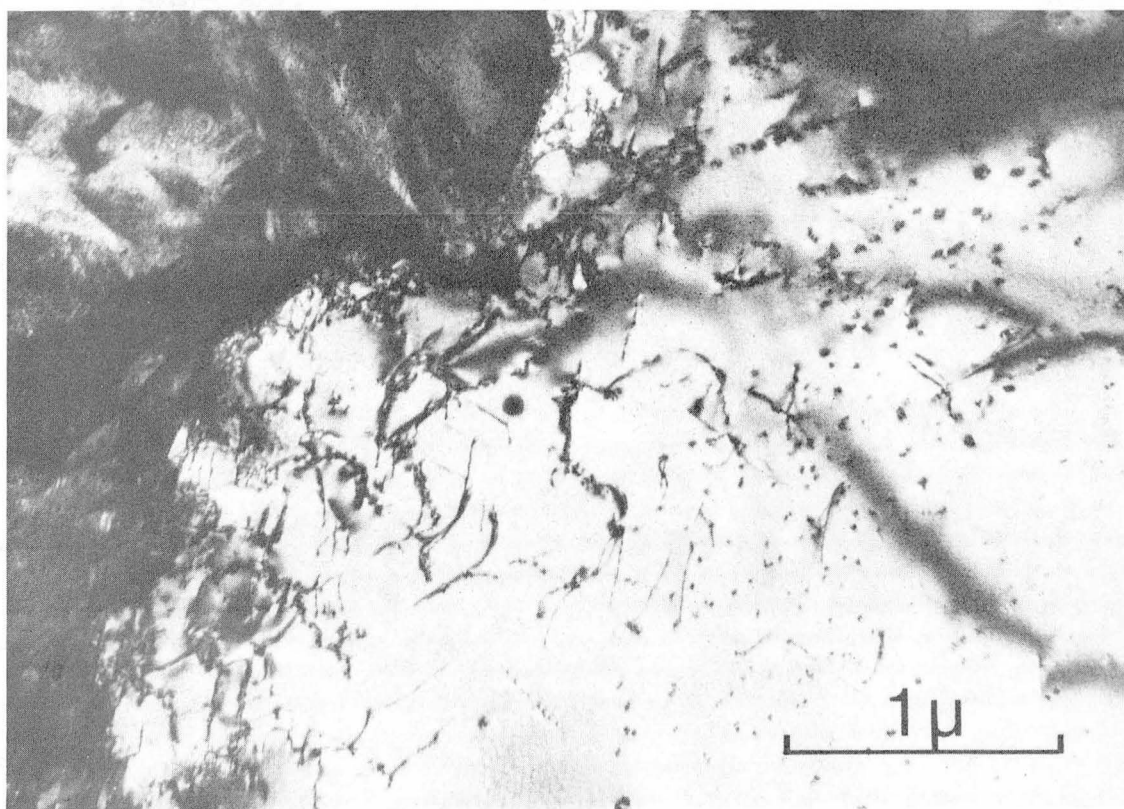
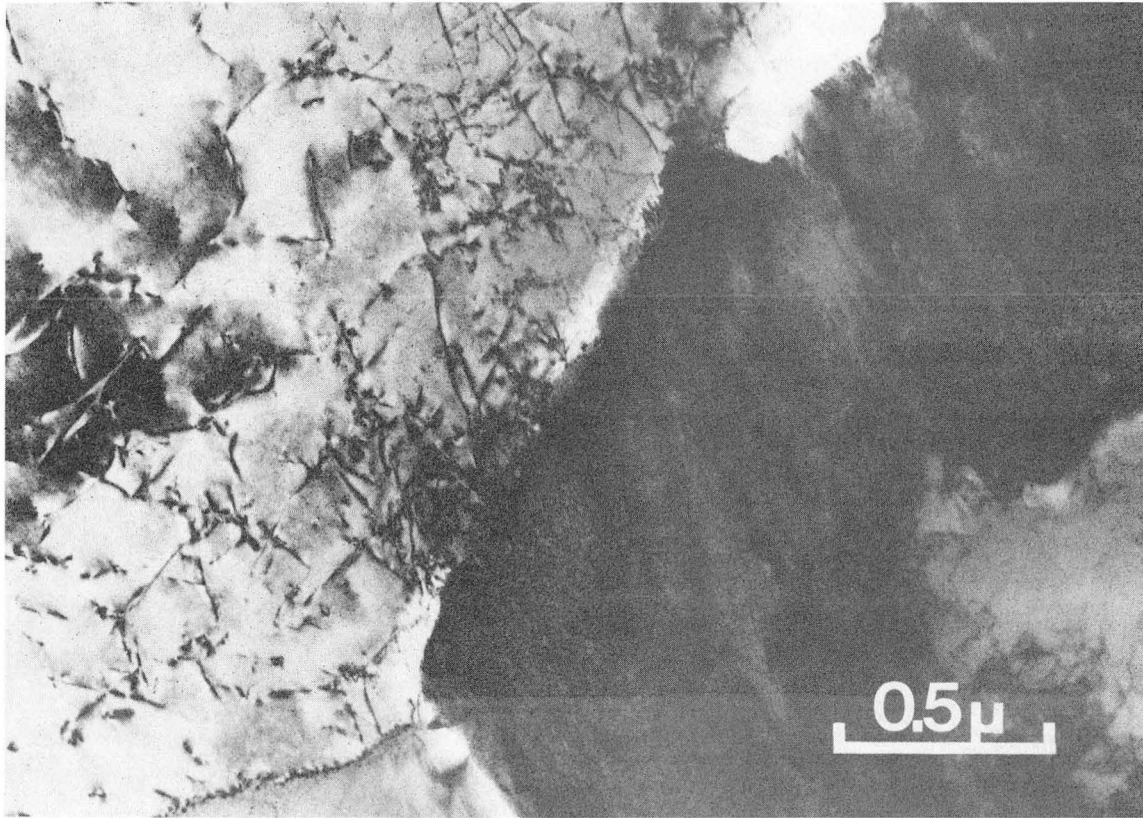


Fig. 4



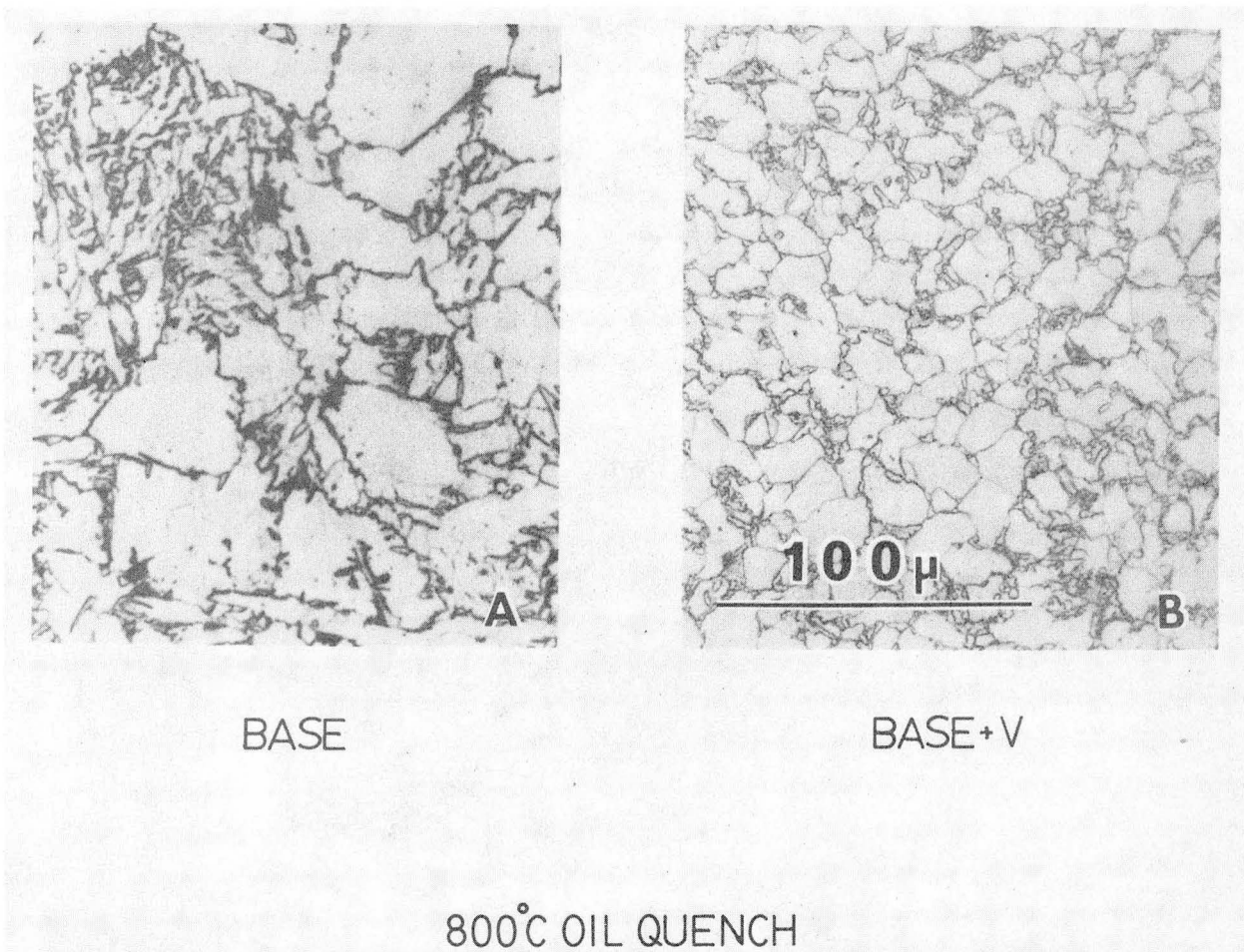
XBB 800-12390

Fig. 5



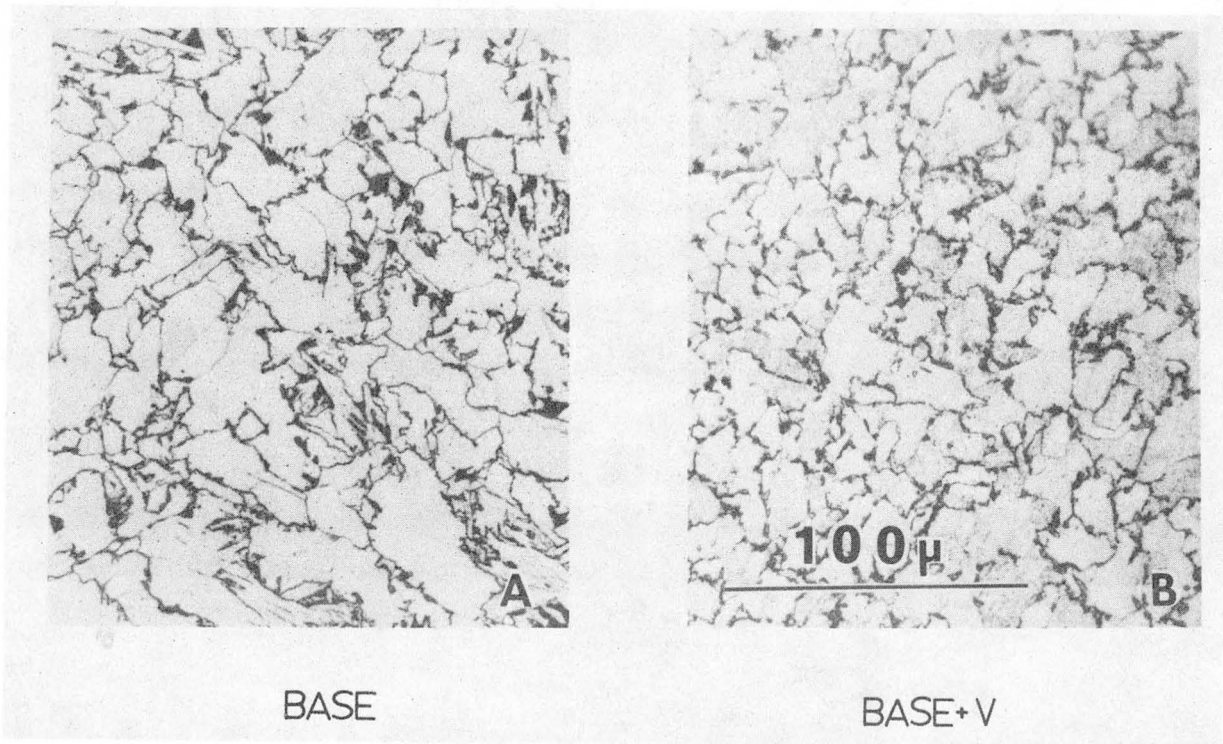
XBB 800-12389

Fig. 6



XBB 800-12385

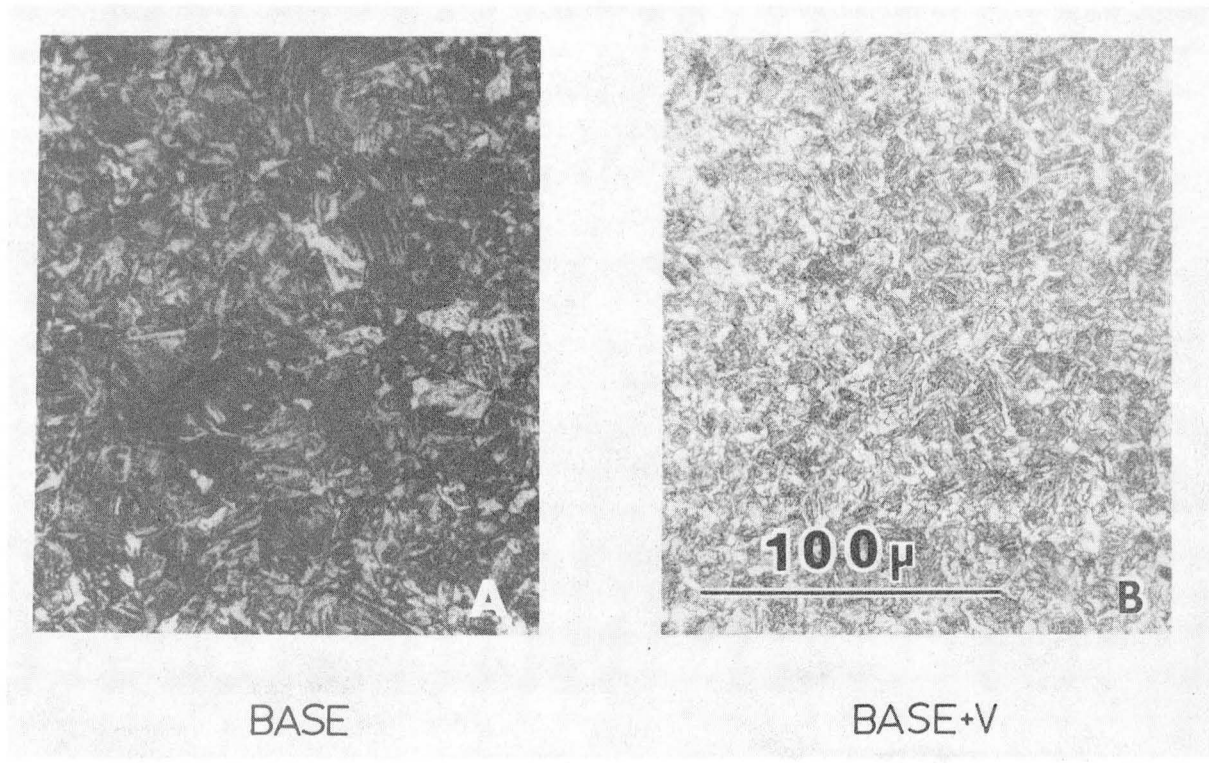
Fig. 7



800°C AIR COOL

XBB 800-12386

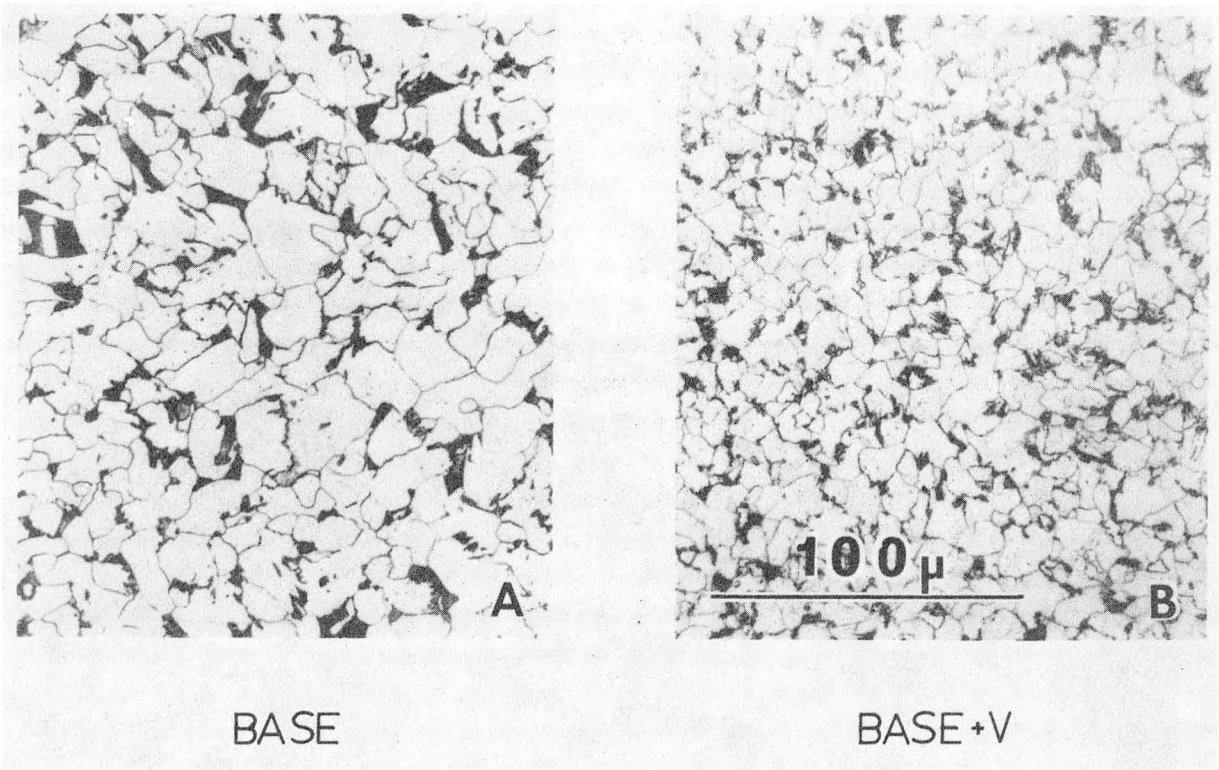
Fig. 8



900°C OIL QUENCH

XBB 800-12388

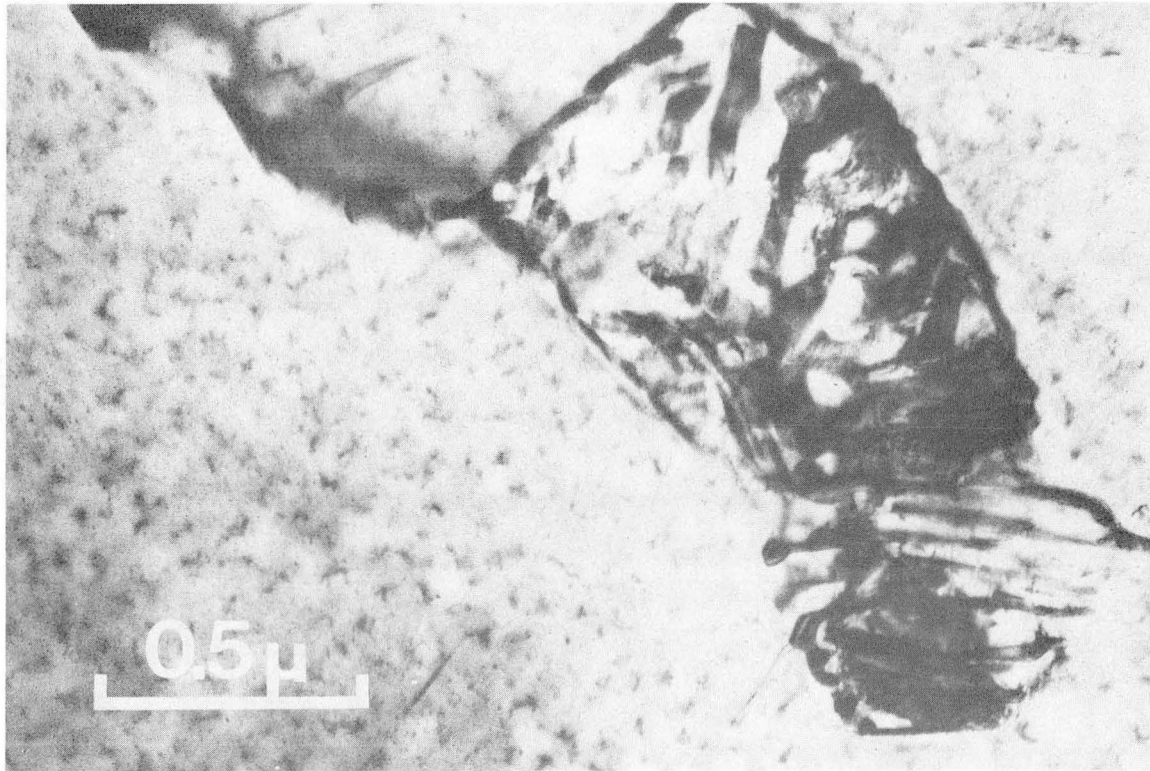
Fig. 9



900°C AIR COOL

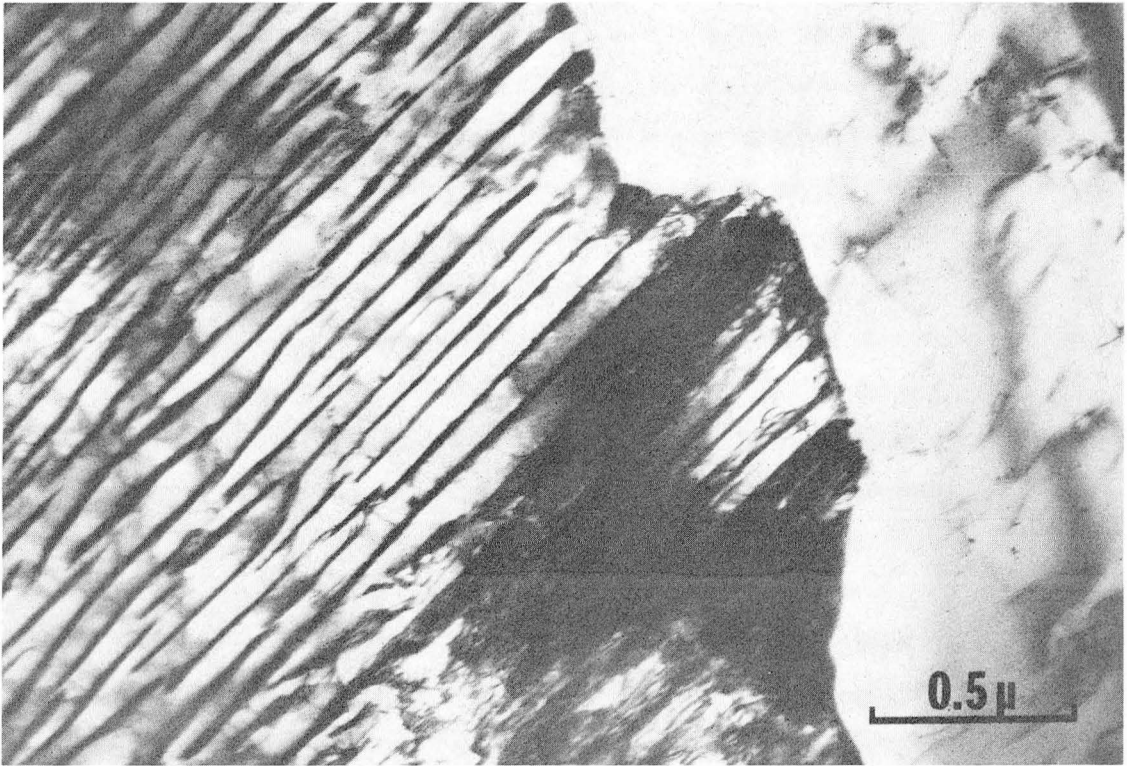
XBB 800-12383

Fig. 11



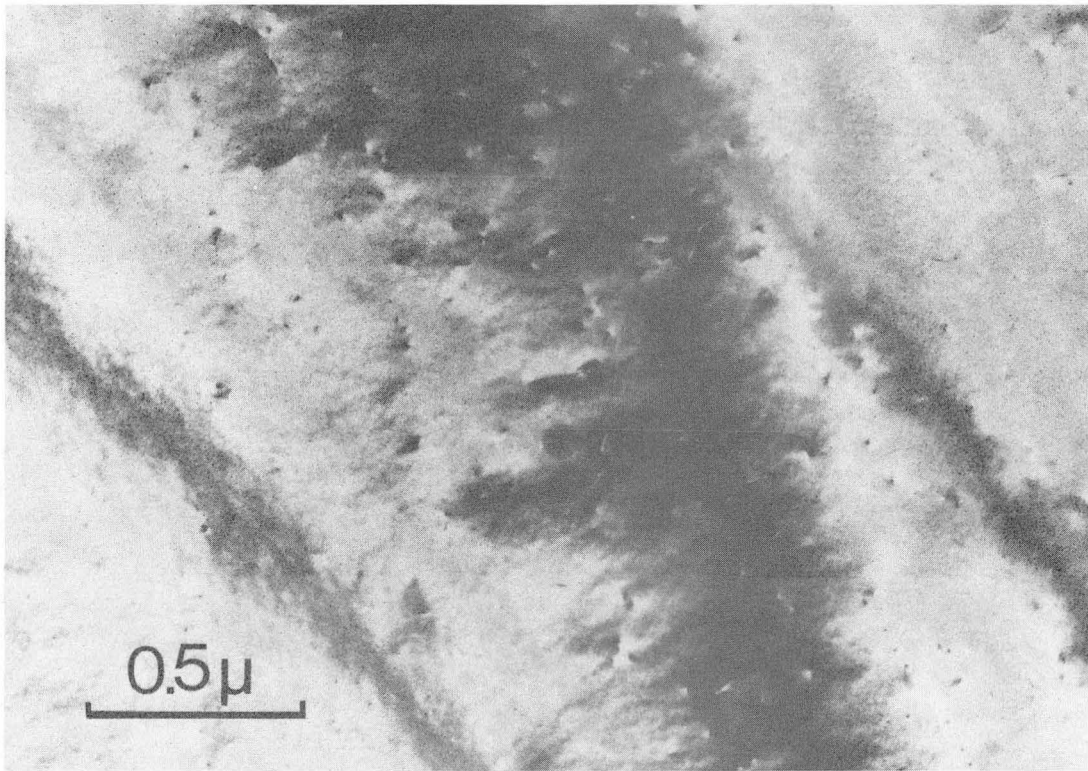
XBB 800-12394

Fig. 12



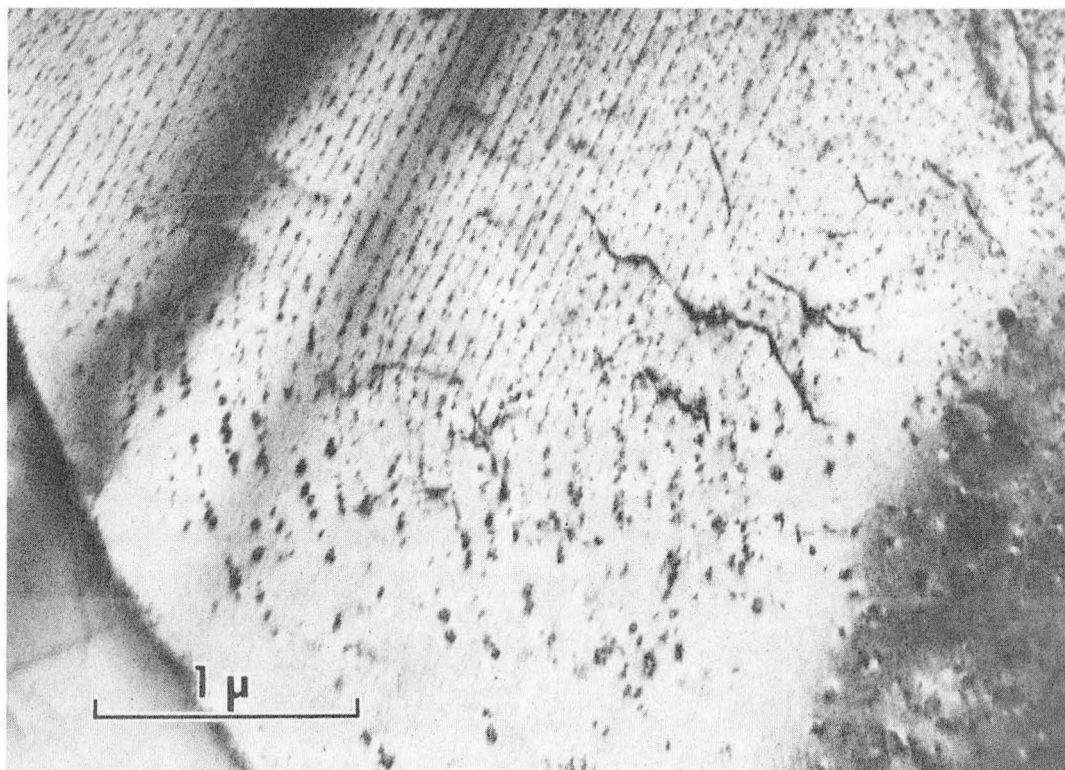
XBB 800-12391

Fig. 13



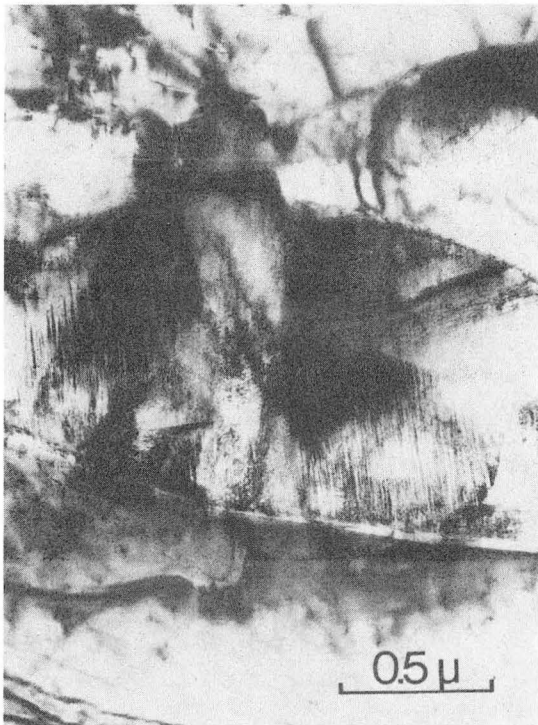
XBB 800-12392

Fig. 14



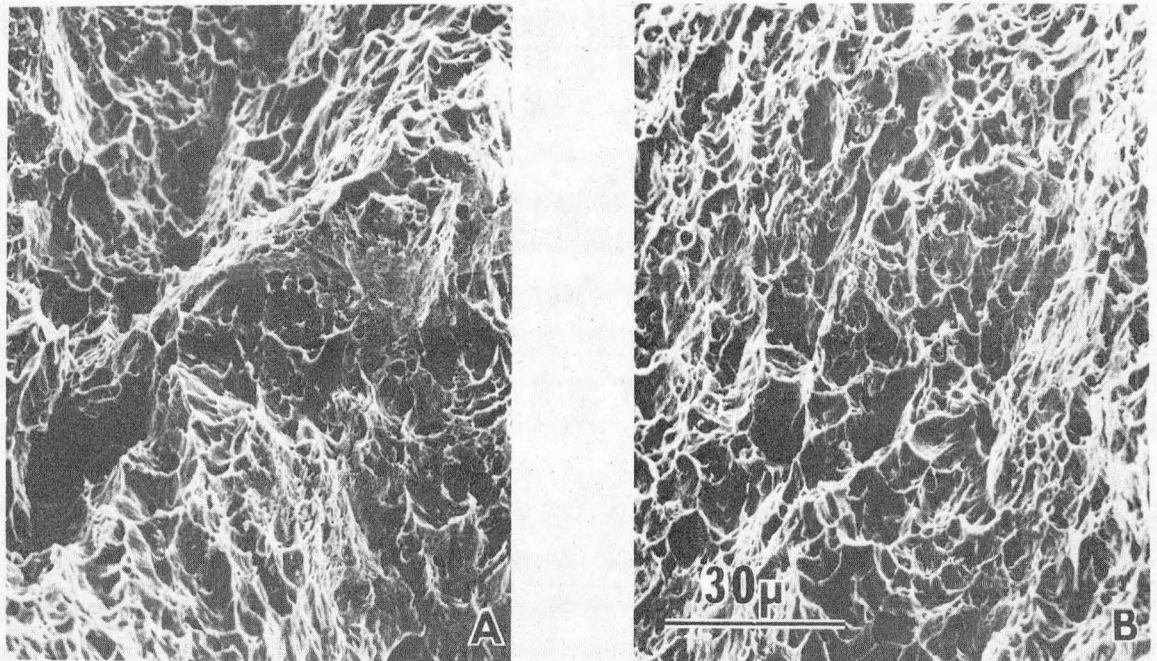
XBB 800-12393

Fig. 15



XBB 800-12395

Fig. 16



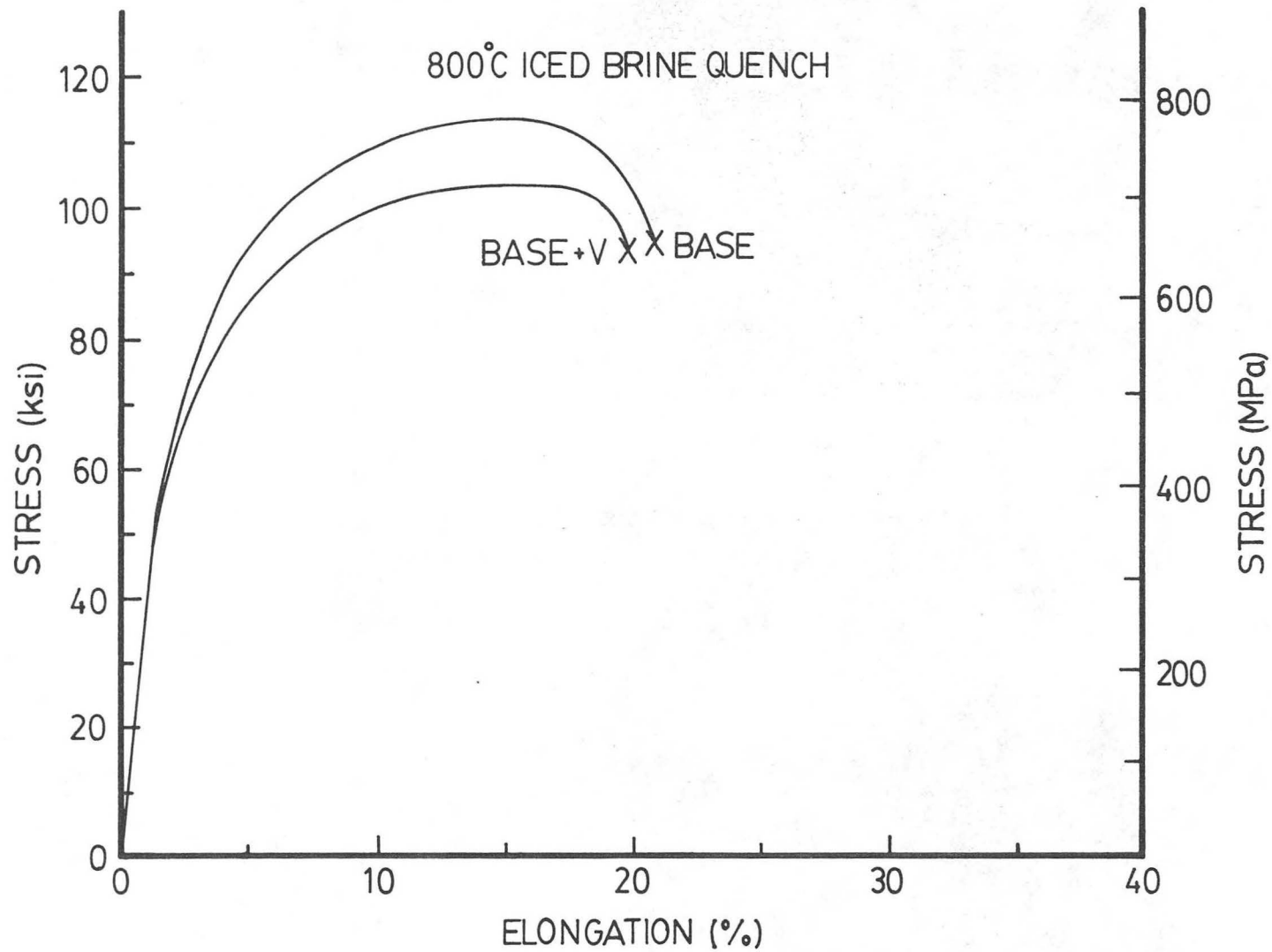
BASE

BASE+V

800°C ICED BRINE QUENCH

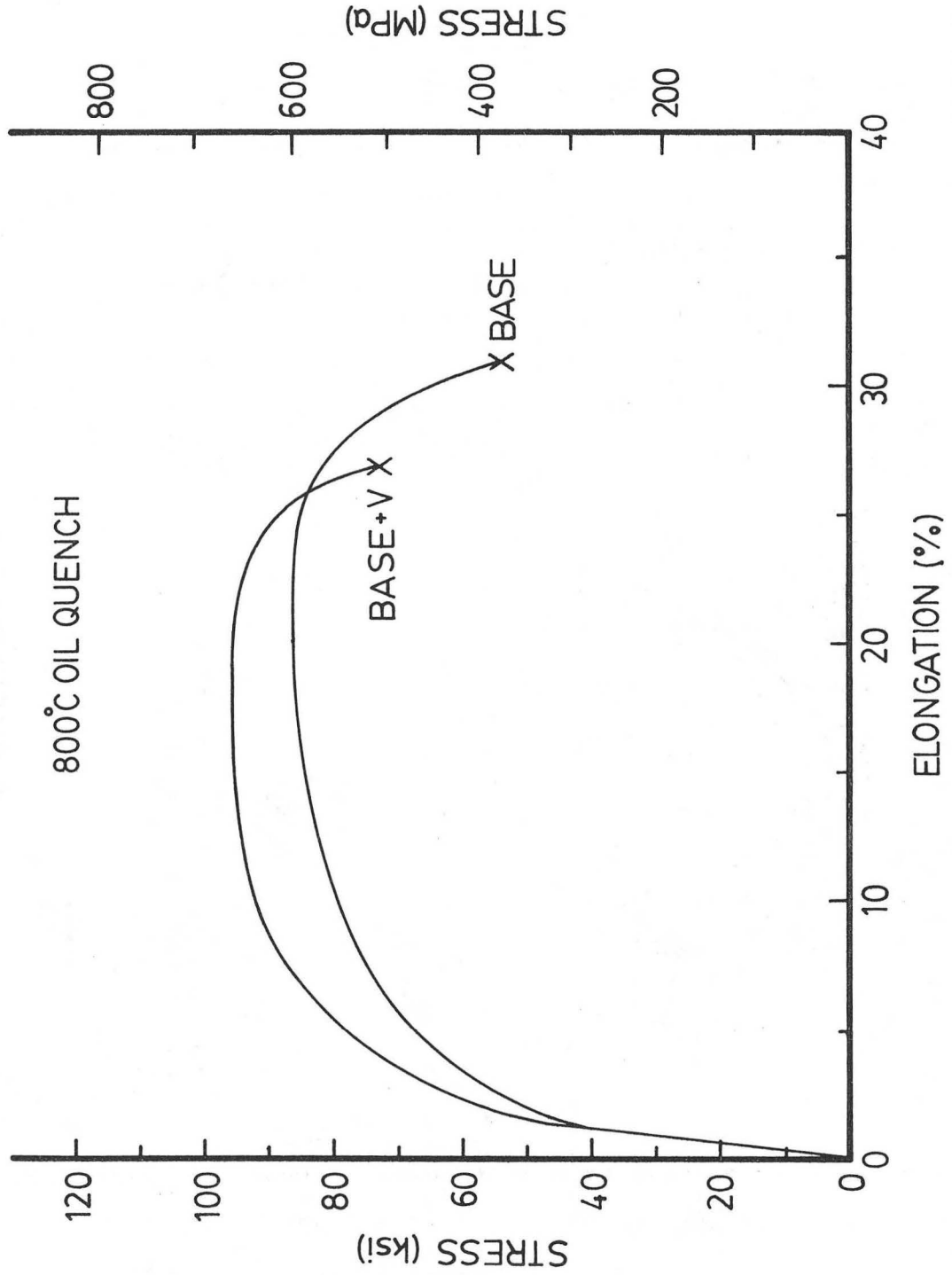
XBB 800-12382

Fig. 17



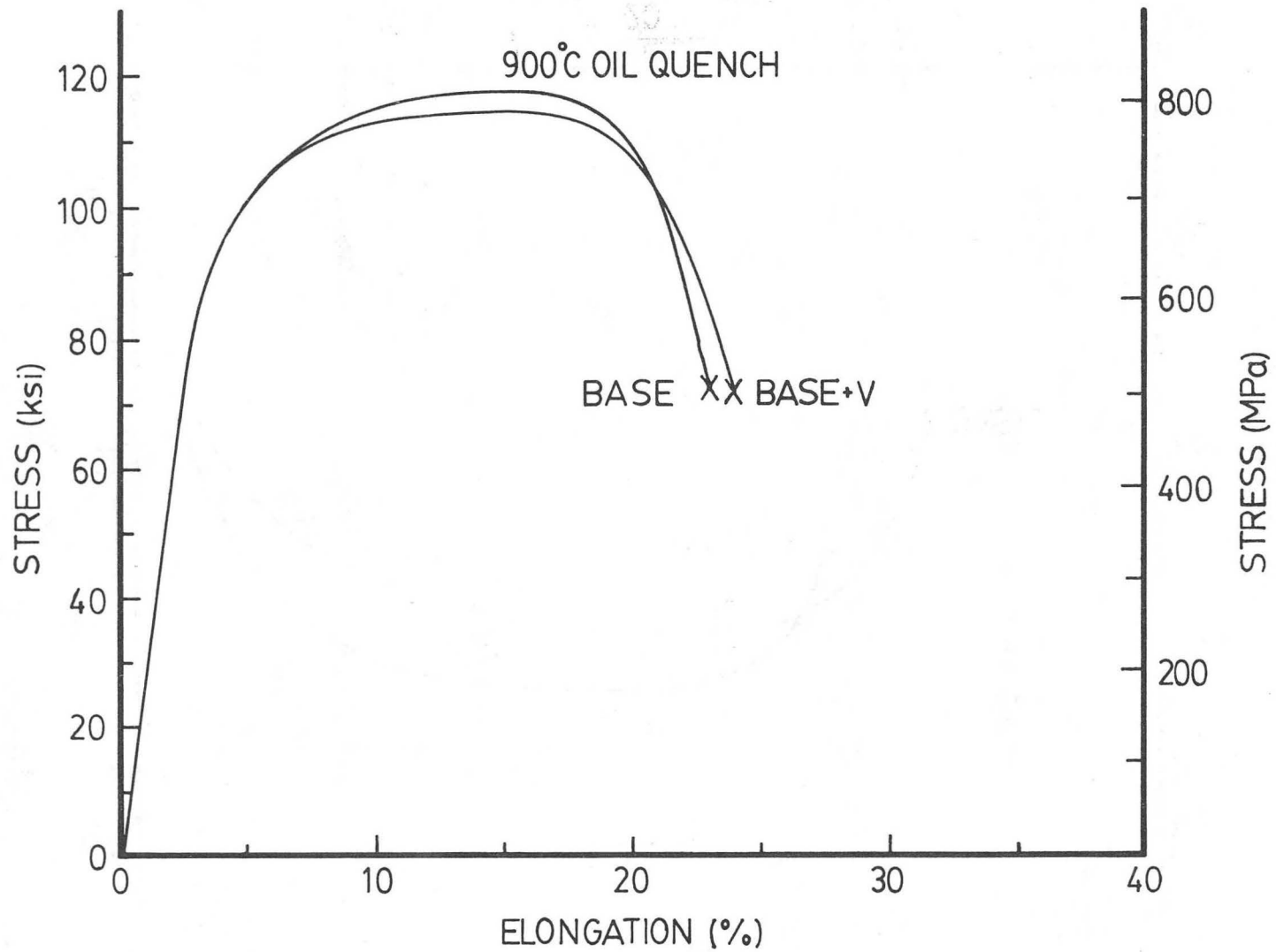
XBL 8011-7408

Fig. 18a



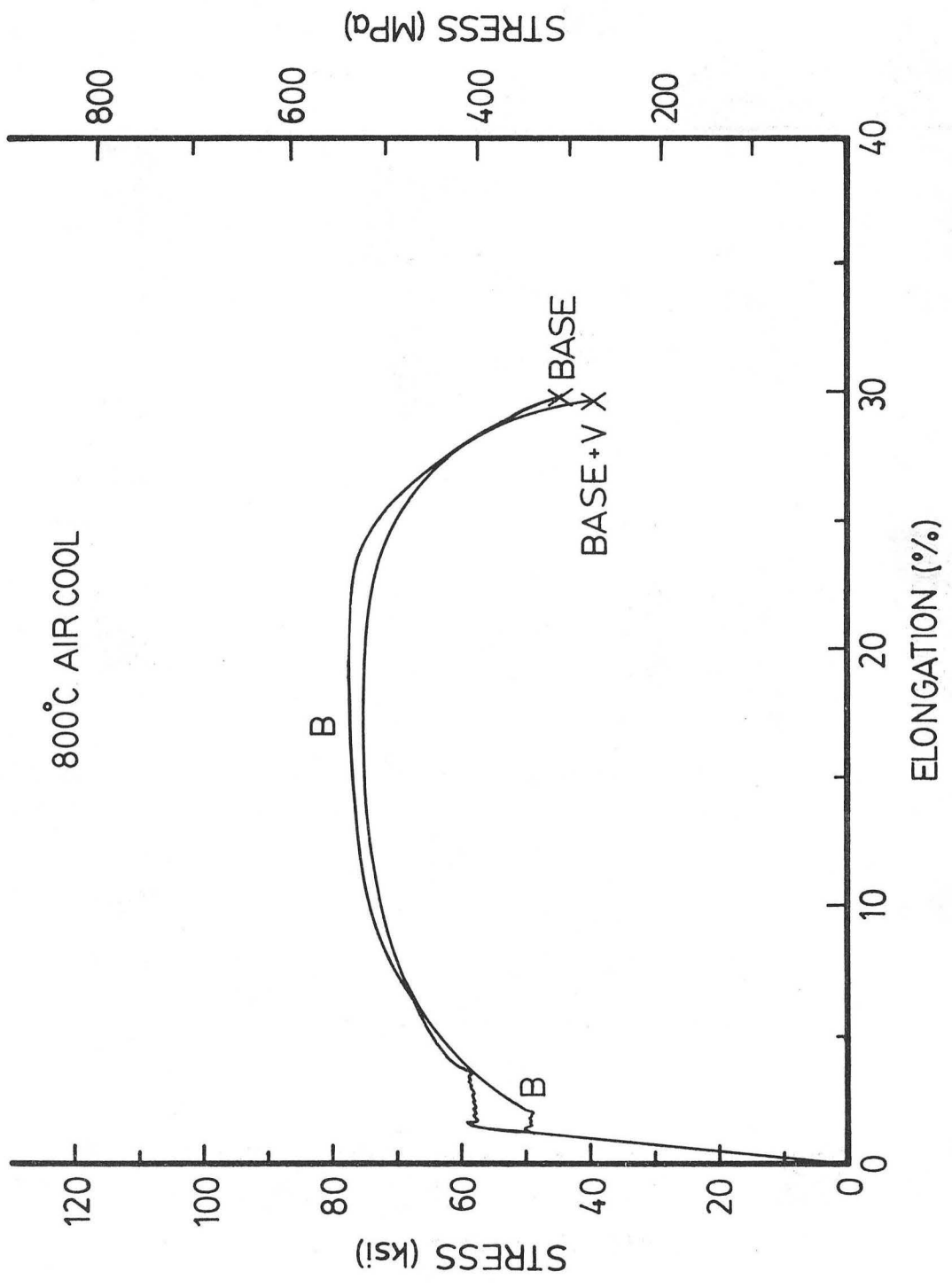
XBL 8011-7411

Fig. 18b



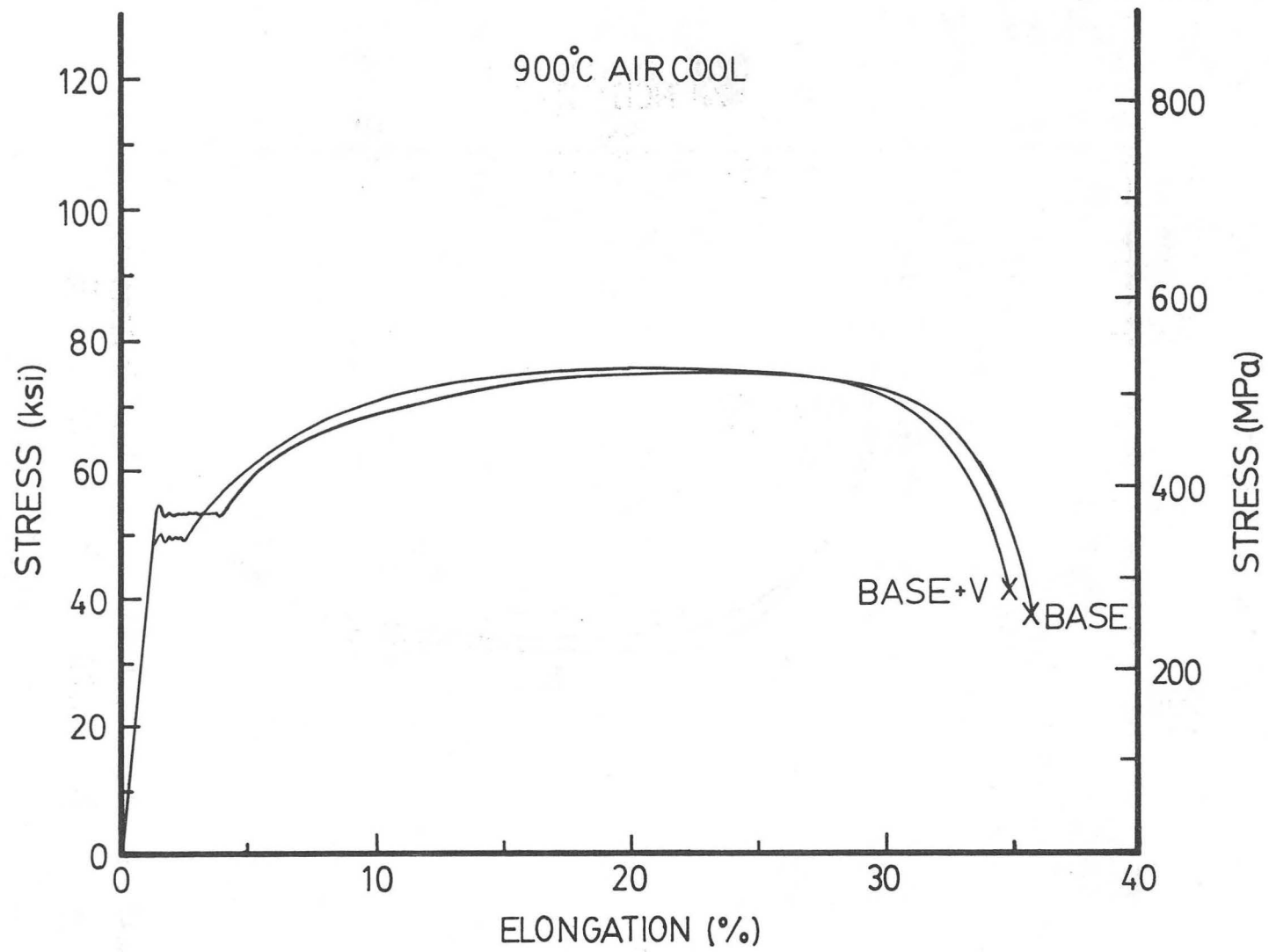
XBL 8011-7412

Fig. 18c



XBL 8011-7407

Fig. 18d



XBL 8011-7410

Fig. 18e

This report was done with support from the Department of Energy. Any conclusions or opinions expressed in this report represent solely those of the author(s) and not necessarily those of The Regents of the University of California, the Lawrence Berkeley Laboratory or the Department of Energy.

Reference to a company or product name does not imply approval or recommendation of the product by the University of California or the U.S. Department of Energy to the exclusion of others that may be suitable.

TECHNICAL INFORMATION DEPARTMENT
LAWRENCE BERKELEY LABORATORY
UNIVERSITY OF CALIFORNIA
BERKELEY, CALIFORNIA 94720